

# Relativistic corrections to double $B_c$ meson production in $e^+e^-$ annihilation\*

Xiao-Peng Wang (王小鹏)<sup>1</sup> Yi-Jie Li (李一杰)<sup>1</sup> Guang-Zhi Xu (许广智)<sup>1†</sup> Kui-Yong Liu (刘魁勇)<sup>2,1‡</sup>

<sup>1</sup>School of Physics, Liaoning University, Shenyang 110036, China

<sup>2</sup>School of Physics and Electronic Technology, Liaoning Normal University, Dalian 116029, China

**Abstract:** Within the framework of nonrelativistic quantum chromodynamics factorization, we investigate relativistic corrections to the production of a pair of  $B_c$  family mesons in  $e^+e^-$  annihilation. The study covers center-of-mass energies from the production threshold up to  $2m_Z$ , considering both the photon and  $Z^0$ -boson propagated processes. We find that the relativistic corrections are significant, with the corresponding  $K$  factors of approximately 0.6. The azimuthal asymmetry, angular distribution, and transverse momentum distribution are also presented.

**Keywords:** NRQCD, relativistic corrections,  $B_c$  meson

**DOI:** 10.1088/1674-1137/ae37f0 **CSTR:** 32044.14.ChinesePhysicsC.50043107

## I. INTRODUCTION

Heavy quarkonia and the  $B_c$  meson, which are bound states of heavy quark pairs ( $c\bar{c}$ ,  $b\bar{b}$ ,  $c\bar{b}$ , and  $b\bar{c}$ ), serve as excellent probes for testing quantum chromodynamics (QCD) and the standard model (SM). Their theoretical description is facilitated by nonrelativistic QCD (NRQCD) factorization formalism [1], which is available because of the large heavy quark mass and small relative velocity between  $Q\bar{Q}$  (or  $Q\bar{Q}'$ ). The pair production of heavy quarkonia in  $e^+e^-$  annihilation provides a crucial testing ground for NRQCD. To match experimental data, both QCD and relativistic corrections are essential [2–9]. Given that  $v^2 \sim \alpha_s$ , these two types of corrections are expected to be comparable in magnitude. Motivated by proposed future high-luminosity  $e^+e^-$  colliders such as the circular electron positron collider (CEPC) [10], future circular collider electron-positron [11], or Z-factory [12], the leading order (LO) and next-to-leading order (NLO) QCD corrections for double heavy quarkonia production at the  $Z^0$  peak have been computed [13–20]. These studies indicate promising detection prospects and reveal that the contributions from color-octet (CO) components and relativistic corrections are also significant [20].

The  $B_c$  meson stands out in the heavy quark bound states family because of its composition of different-flavor quarks and unique weak decay mode. These characteristics provide clearer insights into decay and production mechanisms than those with other quarkonia. Thus far, the only observed ( $b\bar{c}$ ) state is the ground state

$B_c^+(1S)$ , first discovered at the Tevatron in 1998 [21, 22] and later confirmed by large hadron collider (LHC) experiments [23–27], and its excited state  $B_c^+(2S)$ , discovered approximately 15 years later by the ATLAS [28], CMS [29], and LHCb collaborations [30]. Theoretically,  $B_c$  production has been extensively studied across various collision processes. These include direct production in  $e^+e^-$  annihilation (electron production)[31–37] and  $\gamma\gamma$  fusion (photon production) [38–45] at ee colliders;  $gg$  fusion (hadron production) at hadron colliders [41, 46–51];  $\gamma g$  fusion (lepton-hadron production) at ep colliders [52, 53]; production in heavy-ion collisions Pb+Pb at the LHC [54, 55]; and indirect production via the decays of heavy particles such as the  $W$ ,  $Z$ , and Higgs bosons, as well as the top quark [56–66].

The electron-positron production of paired  $B_c$  mesons has been calculated with the collinear factorisation [67]. The LO cross section [17–19, 68], NLO QCD corrections [69] with NRQCD approach, and the relativistic corrections to both the  $s$ -channel single-photon [70] and  $t$ -channel double-photon exchange processes [71] within the relativistic quark model (RQM) have been investigated. However, in contrast to the extensive studies on QCD corrections to  $B_c$  production or the QCD and relativistic corrections to charmonium and bottomonium production, relativistic effects in processes involving  $B_c$  mesons have received comparatively little attention [43, 65, 66, 70–81]. Most existing studies are based on the RQM [43, 65, 66, 70–74, 76], which incorporates relativistic correc-

Received 26 December 2025; Accepted 14 January 2026; Accepted manuscript online 15 January 2026

\* Supported by the National Natural Science Foundation of China (11705078, 12575087)

<sup>†</sup> E-mail: xuguangzhi@lnu.edu.cn

<sup>‡</sup> E-mail: liukuiyong@lnu.edu.cn



Content from this work may be used under the terms of the Creative Commons Attribution 3.0 licence. Any further distribution of this work must maintain attribution to the author(s) and the title of the work, journal citation and DOI. Article funded by SCOAP<sup>3</sup> and published under licence by Chinese Physical Society and the Institute of High Energy Physics of the Chinese Academy of Sciences and the Institute of Modern Physics of the Chinese Academy of Sciences and IOP Publishing Ltd

tions in the amplitude for the heavy quarks' relative motion and in the bound-state wave function. Given that the binding effects are significantly enhanced in pair meson production, we investigate the relativistic corrections for double  $B_c$  production in  $e^+e^-$  annihilation via both  $\gamma^*$  and  $Z^0$  propagators within the NRQCD framework. The specific processes considered are:  $B_c^{*+} + B_c^{*-}$ ,  $B_c^{*+} + B_c^-$ ,  $B_c^+ + B_c^-$ ,  $B_c^{*+} + h_{bc}^-$ ,  $B_c^{*+} + \chi_{bc0}^-$ ,  $B_c^{*+} + \chi_{bc1}^-$ ,  $B_c^{*+} + \chi_{bc2}^-$ ,  $B_c^+ + h_{bc}^-$ ,  $B_c^+ + \chi_{bc0}^-$ ,  $B_c^+ + \chi_{bc1}^-$ ,  $B_c^+ + \chi_{bc2}^-$ .<sup>1)</sup>

The remainder of the paper is organised as follows. In Sec. II, we describe the theoretical framework for the NLO( $v^2$ ) NRQCD calculations. In Sec. III, we present the input parameters used in this work. In Sec. IV, we show the results of the cross-sections, differential cross-sections, and azimuthal asymmetry with and without relativistic corrections. Finally, a brief conclusion is provided in Sec. V.

## II. METHOD OF NRQCD AND RELATIVISTIC CORRECTIONS

Within the NRQCD framework and up-to  $\mathcal{O}(v^2)$ , the production cross-sections are factorized as [1]

$$\begin{aligned} & \hat{\sigma}(e^+ + e^- \rightarrow H_1 + H_2) \\ &= \sum_{n_1, n_2} \left( \frac{F(n_1, n_2)}{m^{d_{\mathcal{O}(n_1)}-4} m^{d_{\mathcal{O}(n_2)}-4}} \langle \mathcal{O}^{H_1}(n_1) \rangle \langle \mathcal{O}^{H_2}(n_2) \rangle \right. \\ &+ \frac{G_1(n_1, n_2)}{m^{d_{\mathcal{P}(n_1)}-4} m^{d_{\mathcal{O}(n_2)}-4}} \langle \mathcal{P}^{H_1}(n_1) \rangle \langle \mathcal{O}^{H_2}(n_2) \rangle \\ &+ \left. \frac{G_2(n_1, n_2)}{m^{d_{\mathcal{O}(n_1)}-4} m^{d_{\mathcal{P}(n_2)}-4}} \langle \mathcal{O}^{H_1}(n_1) \rangle \langle \mathcal{P}^{H_2}(n_2) \rangle \right), \quad (1) \end{aligned}$$

where  $n_1, n_2$  represent the Fock states denoted in spectroscopic notation  $^{2S+1}L_J^{[a]}$ , with total spin  $S$ , orbital angular momentum  $L$ , total angular momentum  $J$ , and color configurations  $a = 1, 8$  corresponding to color-singlet (CS) and CO states, respectively.  $m$  represents the heavy quark effective mass.  $\mathcal{O}^H(n)$  and  $\mathcal{P}^H(n)$  are four-fermion operators of mass dimensions  $d_{\mathcal{O}}$  and  $d_{\mathcal{P}}$  describing the nonperturbative transition  $n \rightarrow H$  at LO and  $\mathcal{O}(v^2)$ .  $\langle \mathcal{O}^H(n) \rangle$  and  $\langle \mathcal{P}^H(n) \rangle$  are the respective long-distance matrix elements (LDMEs), and  $F(n_1, n_2)$  and  $G_i(n_1, n_2)$  are the appropriate short-distance-coefficients (SDCs). The SDCs describe the short-distance production of two Fock states  $(c\bar{b})[n_1]$  and  $(b\bar{c})[n_2]$ , and the LDMEs describe the hadronization of the Fock state  $n_{1,2}$  into the physical  $B_c$  mesons  $H_{1,2}$ . The SDCs are perturbatively calculable and the LDMEs can be obtained by the potential model [82–84] and potential NRQCD [85].

In the subsequent discussion, we see that the contribution of the CO channels for double  $B_c$  production is negligible compared to that of the CS channels. Within the CS framework, the relevant four-quark operators for the pro-

duction of  $H = B_c, B_c^*, \dots$  are defined as [1] (for simplicity, only the  $S$ -wave operators are listed herein).

$$\begin{aligned} \mathcal{O}^H(^1S_0^{[1]}) &= \chi^\dagger \psi(a_H^\dagger a_H) \psi^\dagger \chi, \\ \mathcal{P}^H(^1S_0^{[1]}) &= \frac{1}{2} [\chi^\dagger \psi(a_H^\dagger a_H) \psi^\dagger \left( -\frac{i}{2} \overleftrightarrow{\mathbf{D}} \right)^2 \chi + \text{h.c.}], \\ \mathcal{O}^H(^3S_1^{[1]}) &= \chi^\dagger \sigma^i \psi(a_H^\dagger a_H) \psi^\dagger \sigma^i \chi, \\ \mathcal{P}^H(^3S_1^{[1]}) &= \frac{1}{2} \left[ \chi^\dagger \sigma^i \psi(a_H^\dagger a_H) \psi^\dagger \sigma^i \left( -\frac{i}{2} \overleftrightarrow{\mathbf{D}} \right)^2 \chi + \text{h.c.} \right], \quad (2) \end{aligned}$$

where  $\psi(\chi)$  represents the Pauli spinor that annihilates (creates) a heavy quark (antiquark),  $\sigma^i (i=1, 2, 3)$  are the Pauli matrices, and  $\overleftrightarrow{\mathbf{D}} = \overrightarrow{\mathbf{D}} - \overleftarrow{\mathbf{D}}$ , with  $\overrightarrow{\mathbf{D}}$  being the space component of the covariant derivative  $D^\mu$ .

For  $S$  and  $P$  wave states, the LDMEs at LO are related to the values of radial functions and the first derivatives of radial functions at the origin,

$$\begin{aligned} \frac{\langle \mathcal{O}^{B_c^*}(^3S_1^{[1]}) \rangle}{2N_c \times 3} &= \frac{|R_S(0)|^2}{4\pi}, \quad \frac{\langle \mathcal{O}^{B_c}(^1S_0^{[1]}) \rangle}{2N_c} = \frac{|R_S(0)|^2}{4\pi}, \\ \frac{\langle \mathcal{O}^{h_{bc}}(^3P_J^{[1]}) \rangle}{2N_c \times (2J+1)} &= \frac{3|R'_P(0)|^2}{4\pi}, \quad \frac{\langle \mathcal{O}^{h_{bc}}(^1P_1^{[1]}) \rangle}{2N_c \times 3} = \frac{3|R'_P(0)|^2}{4\pi}. \quad (3) \end{aligned}$$

It is convenient to define matrix elements  $\langle v^2 \rangle$  instead of the LDMEs at  $\mathcal{O}(v^2)$  [86–88].

$$\langle v^2 \rangle \equiv \frac{\langle \mathcal{P}^H(n) \rangle}{m^2 \langle \mathcal{O}^H(n) \rangle}. \quad (4)$$

The SDCs can be obtained via the matching condition between perturbative QCD and NRQCD calculations.

$$\begin{aligned} & \hat{\sigma}(e^+ + e^- \rightarrow (c\bar{b})_1 + (b\bar{c})_2) \Big|_{\text{pert QCD}} \\ &= \left[ \frac{F(n_1, n_2)}{m^{d_{\mathcal{O}(n_1)}-4} m^{d_{\mathcal{O}(n_2)}-4}} \langle 0 | \mathcal{O}^{(c\bar{b})_1}(n_1) | 0 \rangle \langle 0 | \mathcal{O}^{(b\bar{c})_2}(n_2) | 0 \rangle \right. \\ &+ \frac{G_1(n_1, n_2)}{m^{d_{\mathcal{P}(n_1)}-4} m^{d_{\mathcal{O}(n_2)}-4}} \langle 0 | \mathcal{P}^{(c\bar{b})_1}(n_1) | 0 \rangle \langle 0 | \mathcal{O}^{(b\bar{c})_2}(n_2) | 0 \rangle \\ &+ \left. \frac{G_2(n_1, n_2)}{m^{d_{\mathcal{O}(n_1)}-4} m^{d_{\mathcal{P}(n_2)}-4}} \langle 0 | \mathcal{O}^{(c\bar{b})_1}(n_1) | 0 \rangle \langle 0 | \mathcal{P}^{(b\bar{c})_2}(n_2) | 0 \rangle \right] \Big|_{\text{pert NRQCD}}. \quad (5) \end{aligned}$$

The left-hand side of Eq. (5) can be computed easily by using the covariant projection method [86].

The Feynman diagrams for the exclusive  $B_c$  pair production  $e^-e^+ \rightarrow \gamma^*/Z^0 \rightarrow H_1^+(p_1) + H_2^-(p_2)$  are displayed in Fig. 1. Here, we only present diagrams for  $s$ -channel processes. The  $t$ -channel double-photon fragmentation mechanism dominates the production of  $J/\psi$  and  $\Upsilon$  pairs [20, 89, 90], as the photon can fragment into a  $^3S_1$  quarkonium state. In contrast, similar to the case of  $\eta_{c/b}$  pair production where the photon cannot fragment into a  $^1S_0$  state

1) Processes related by charge conjugation, such as  $B_c^{*+} + B_c^-$  and  $B_c^+ + B_c^{*-}$ , have identical cross sections.

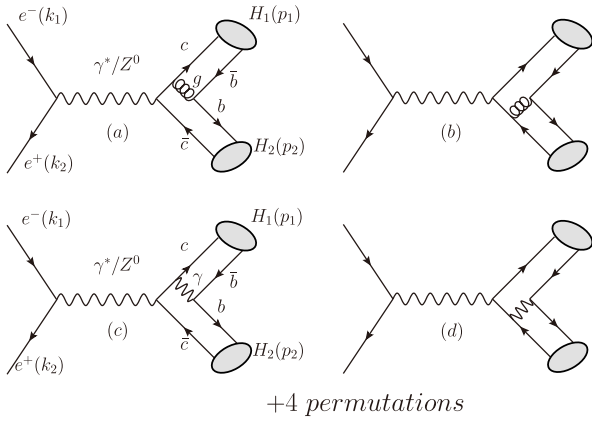


**Fig. 1.** Feynman diagrams for  $e^-(k_1) + e^+(k_2) \rightarrow \gamma^*/Z^0 \rightarrow H_1(p_1) + H_2(p_2)$  at the tree level.  $H_1, H_2$  are  $B_c^+(c\bar{b})$  and  $B_c^-(b\bar{c})$  (or their respective excited states,  $B_c^{*+}, h_{bc}^+, \chi_{bcJ}^+(J=0,1,2)$ ), respectively. The permutation diagrams can be obtained by reversing the quark lines and exchanging  $b, c$  quarks. (a) and (b) diagrams belonging to QCD channels, (c) and (d) diagrams belonging to EW channels.

because of  $C$ -parity conservation, that of the  $B_c$  pair production proceeds only via the non-fragmentation mechanism because a photon cannot fragment into a  $c\bar{b}$  quark pair. Subsequent calculations indicate that the  $t$ -channel contributions are negligible. In the diagrams,  $H_1$  and  $H_2$  are the positively and negatively charged  $B_c$  mesons, with the quark contents of  $c(p_c)\bar{b}(p_{\bar{b}})$  and  $b(p_b)\bar{c}(p_{\bar{c}})$ , respectively. The momenta of the heavy quarks in the mesons are defined as

$$\begin{aligned} p_c &= \frac{E_c}{E_c + E_{\bar{b}}} p_1 + q_1, \\ p_{\bar{b}} &= \frac{E_{\bar{b}}}{E_c + E_{\bar{b}}} p_1 - q_1, \\ p_b &= \frac{E_b}{E_{\bar{c}} + E_b} p_2 + q_2, \\ p_{\bar{c}} &= \frac{E_{\bar{c}}}{E_{\bar{c}} + E_b} p_2 - q_2, \end{aligned} \quad (6)$$

$E_{c/\bar{b}} = \sqrt{m_{c/\bar{b}}^2 + \vec{q}_1^2}$  and  $E_{b/\bar{c}} = \sqrt{m_{b/\bar{c}}^2 + \vec{q}_2^2}$  are the energies of constituent quarks in the rest frame of the meson, where  $\vec{q}_i (i=1,2)$  represent the three-momenta of the quarks; each can be expressed as the product of the reduced mass  $\mu_H = \frac{m_c m_b}{m_c + m_b}$  and effective quark velocity  $\vec{v}$ . Meanwhile,  $q_i$  represents the corresponding four-momenta subject to constraints  $q_i \cdot p_i = 0$ .

$$|\vec{q}_i| = 2\mu_H v_i. \quad (7)$$

1) These normalization factors will be  $\sqrt{2m_1(E_c + E_{\bar{b}})}$  and  $\sqrt{2m_2(E_b + E_{\bar{c}})}$  when Dirac spinors are normalized as  $u^\dagger u = v^\dagger v = 1$ , and the projection operator in Eq. (9) is divided by a factor of  $2\sqrt{E_c E_{\bar{b}}}$  [77–79, 81, 86].

The full QCD scattering amplitude may be written as

$$\begin{aligned} A(q_1, q_2) &= \sum_{s_c, s_{\bar{b}}} \sum_{s_c, s_b} \sum_{k_1 l_1} \langle s_c; s_{\bar{b}} | S_1 S_{1z} \rangle \langle 3, k_1; \bar{3}, l_1 | 1 \rangle \\ &\times \langle s_{\bar{c}}; s_b | S_2 S_{2z} \rangle \langle 3, k_2; \bar{3}, l_2 | 1 \rangle \\ &\times \mathcal{A}(e^+ + e^- \rightarrow c_{k_1} + \bar{b}_{l_1} + b_{k_2} + \bar{c}_{l_2}), \end{aligned} \quad (8)$$

where  $\mathcal{A}(e^+e^- \rightarrow c + \bar{b} + b + \bar{c})$  represents the standard Feynman amplitude. In addition, the Breit-Wigner formula is utilized for the  $Z^0$  propagator within the amplitudes [13, 17–20], namely  $\mathcal{D}_{\mu\nu} = \frac{-ig_{\mu\nu}}{p^2 - m_Z^2 + im_Z \Gamma_Z}$ . The covariant projector method is employed in the calculations [7, 20, 77–79, 81, 88, 91–94]. The projector operator for  $H_1$  in the spin-triplet state is given by

$$\begin{aligned} \mathbb{P}_1 &= \sum_{s_c, s_{\bar{b}}} \sum_{kl} \langle 3, k; \bar{3}, l | 1 \rangle \langle s_c; s_{\bar{b}} | 1 S_z \rangle v_l(p_{\bar{b}}; s_{\bar{b}}) \bar{u}_k(p_c; s_c) \\ &= \frac{1}{2\sqrt{2}\sqrt{E_c + m_c}\sqrt{E_{\bar{b}} + m_b}} (-\not{p}_{\bar{b}} + m_b) \\ &\times \not{\epsilon}_{S_z} \frac{\not{p}_c + \not{p}_{\bar{b}} + E_c + E_{\bar{b}}}{E_c + E_{\bar{b}}} (\not{p}_c + m_c) \otimes \left( \frac{\mathbf{1}_c}{\sqrt{N_c}} \right), \end{aligned} \quad (9)$$

with the Dirac spinors normalized as  $\bar{u}u = 2m_c$  and  $-\bar{v}v = 2m_b$ . Here,  $\epsilon_{S_z}$  represents a unit spin polarization vector. For the spin-singlet state, the spin state  $|1S_z\rangle$  is replaced by  $|00\rangle$ , and  $\not{\epsilon}_{S_z}$  is replaced by  $\gamma_5$ . The expression  $\langle 3, k; \bar{3}, l | 1 \rangle = \frac{\delta_{kl}}{\sqrt{N_c}} = \frac{\mathbf{1}_c}{\sqrt{N_c}}$  corresponds to the Clebsch-Gordan coefficient in the  $SU(3)$  color space, which projects the  $(b\bar{c})$  pair onto the CS state  $|1\rangle$ . Here,  $\mathbf{1}_c$  represents the unit color matrix and  $N_c$  denotes the number of colors in QCD. The projector operator for  $H_2$  can be obtained by making the following replacements in Eq. (9):  $\bar{b} \rightarrow \bar{c}$ ,  $c \rightarrow b$ , and  $m_c \leftrightarrow m_b$ . The complete color factor for QCD diagrams (a, b) is  $\frac{N_c^2 - 1}{2N_c} = C_F$ ; pure EW diagrams (c, d), 1; and  $t$ -channel double photon exchange processes discussed in Sec. IV A, 1.

To expand Eq. (8) as a double series in  $q_1$  and  $q_2$ , it is convenient to define

$$A_{\alpha_1 \dots \alpha_m, \beta_1 \dots \beta_n} = \sqrt{\frac{m_1}{E_1}} \sqrt{\frac{m_2}{E_2}} \left[ \frac{\partial^{m+n} A(q_1, q_2)}{\partial q_1^{\alpha_1} \dots \partial q_1^{\alpha_m} \partial q_2^{\beta_1} \dots \partial q_2^{\beta_n}} \Big|_{q_1=q_2=0} \right], \quad (10)$$

where the factor  $\sqrt{m_i/E_i}$  compensates the relativistic normalization<sup>1)</sup> of the  $(bc)_i$  pair with  $m_1 = m_2 = 2\mu_H$ ,  $E_1 = 2E_c E_{\bar{b}} / (E_c + E_{\bar{b}})$ ,  $E_2 = 2E_b E_{\bar{c}} / (E_b + E_{\bar{c}})$ . Such that

$$A(q_1, q_2) = A_{0,0} + q_1^{\alpha_1} A_{\alpha_1,0} + q_2^{\beta_1} A_{0,\beta_1} + \frac{1}{2} q_1^{\alpha_1} q_1^{\alpha_2} A_{\alpha_1\alpha_2,0} + \frac{1}{2} q_2^{\beta_1} q_2^{\beta_2} A_{0,\beta_1\beta_2} + \dots \quad (11)$$

Here, the subscript "0" means no derivatives of  $q_i$  to the amplitude.

For  $S$ -wave states, only even powers of  $q_i$  contribute in the expansion. The following replacement is adopted in our calculations [7, 91]:

$$q_i^\mu q_i^\nu \rightarrow \frac{|\vec{q}_i|^2}{3} \Pi_i^{\mu\nu}, \quad (12)$$

with  $\Pi_i^{\mu\nu} = -g^{\mu\nu} + \frac{p_i^\mu p_i^\nu}{p_i^2}$ . For  $P$ -wave states, only odd powers of  $q_i$  contribute. The corresponding replacements are given as [92–94]

$$q_i^\mu \rightarrow |\vec{q}_i| \epsilon_{L_c}^\mu(p_i) \\ q_i^\mu q_i^\nu q_i^\xi \rightarrow \frac{|\vec{q}_i|^3}{5} \Pi_i^{\mu\nu\xi} = \frac{|\vec{q}_i|^3}{5} (\Pi_i^{\mu\nu} \epsilon_{L_c}^\xi + \Pi_i^{\nu\xi} \epsilon_{L_c}^\mu + \Pi_i^{\xi\mu} \epsilon_{L_c}^\nu), \quad (13)$$

where  $\epsilon_{L_c}(p_i)$  represents the orbital polarization vector of the  $P$ -wave meson. For the  $^3S_1$  and  $^1P_1$  states, because the total angular momentum polarization vector equals the spin or orbital polarization vector, the corresponding polarization sum relationships are expressed as

$$\sum_{J_z} \epsilon_{L_c}^\mu \epsilon_{L_c}^\nu = \Pi_i^{\mu\nu}. \quad (14)$$

For  $^3P_J$  states ( $J=0,1,2$ ), spin and orbital polarization vectors couple to generate the specific total angular momentum polarization, which can be expressed as

$$\sum_{L_c S_z} \epsilon_{L_c}^\mu \epsilon_{S_z}^\nu \langle 1L_c; 1S_z | J, J_z \rangle = \epsilon^{\mu\nu}(J, J_z). \quad (15)$$

Upon summing over  $J_z$ , the relevant polarization sum relationships are listed below [95].

$$\begin{aligned} \epsilon^{\mu\nu}(0, J_z) \epsilon^{*\mu'\nu'}(0, J_z) &= \frac{1}{3} \Pi_i^{\mu\nu} \Pi_i^{\mu'\nu'}, \\ \sum_{J_z} \epsilon^{\mu\nu}(1, J_z) \epsilon^{*\mu'\nu'}(1, J_z) &= \frac{1}{2} (\Pi_i^{\mu\mu'} \Pi_i^{\nu\nu'} - \Pi_i^{\mu\nu'} \Pi_i^{\mu'\nu}), \\ \sum_{J_z} \epsilon^{\mu\nu}(2, J_z) \epsilon^{*\mu'\nu'}(2, J_z) &= \frac{1}{2} (\Pi_i^{\mu\mu'} \Pi_i^{\nu\nu'} + \Pi_i^{\mu\nu'} \Pi_i^{\mu'\nu}) - \frac{1}{3} \Pi_i^{\mu\nu} \Pi_i^{\mu'\nu'}. \end{aligned} \quad (16)$$

As for the kinematics, the Mandelstam variables are

defined as

$$s = (k_1 + k_2)^2, t = (k_1 - p_1)^2, u = (k_1 - p_2)^2, \quad (17)$$

$t, u$  depend on  $|\vec{q}_i|^2$ . We define  $t_0, u_0$  as values at  $|\vec{q}_i|^2 = 0$  (non-relativistic result); therefore,  $t, u$  are expanded up-to  $O(v^2)$  as

$$t = t_0 + \frac{t_0 + M^2}{4M^2 - s} \frac{M^2}{m_c m_b} (|\vec{q}_1|^2 + |\vec{q}_2|^2) + O(v^4), \quad (18)$$

$$u = u_0 + \frac{u_0 + M^2}{4M^2 - s} \frac{M^2}{m_c m_b} (|\vec{q}_1|^2 + |\vec{q}_2|^2) + O(v^4), \quad (19)$$

where  $M = m_c + m_b$ . The master formulas for the SDCs in the matching condition of Eq. (5) are given by

$$\frac{F(n_1, n_2)}{m^4} = \frac{1}{8s} \int \sum |\mathcal{M}|^2 d\phi_2^{(0)}, \quad (20)$$

$$\frac{G_1(n_1, n_2)}{m^6} = \frac{1}{8s} \int (f_{ps} * \sum |\mathcal{M}|^2 + \sum |N_1|^2) d\phi_2^{(0)}, \quad (21)$$

$$\frac{G_2(n_1, n_2)}{m^6} = \frac{1}{8s} \int (f_{ps} * \sum |\mathcal{M}|^2 + \sum |N_2|^2) d\phi_2^{(0)}, \quad (22)$$

where  $|\mathcal{M}|^2, |N_i|^2$  denote the amplitudes squared at  $O(v^0)$  and  $O(v^2)$ , respectively.  $1/(8s)$  is the flux factor  $1/(2s)$  multiplied by the spin-average factor  $1/4$  for the initial electron-positron pair.  $d\phi_2^{(0)}$  is the two-body phase space integral element at  $O(v^0)$ , and  $f_{ps} = -\frac{r}{m_c m_b (1-4r)}$  with  $r = (m_c + m_b)^2/s$  comes from the relativistic expansion to the phase space factor<sup>1)</sup>. The amplitudes squared are explicitly expressed as below

$$|\mathcal{M}|^2 = \begin{cases} |A_{0,0}|^2 \Big|_{\vec{q}_1^2 = \vec{q}_2^2 = 0}, \\ \epsilon_{L_c}^{*\beta'_1} \epsilon_{L_c}^{\beta_1} A_{0,\beta'_1}^* A_{0,\beta_1} \Big|_{\vec{q}_1^2 = \vec{q}_2^2 = 0}, \end{cases} \quad (23)$$

$$|N_1|^2 = \begin{cases} \left[ \frac{\partial}{\partial \vec{q}_1^2} (|A_{0,0}|^2) + \frac{1}{3} \Pi_1^{\alpha_1 \alpha_2} \text{Re} [A_{0,0}^* A_{\alpha_1 \alpha_2, 0}] \right] \Big|_{\vec{q}_1^2 = \vec{q}_2^2 = 0}, \\ \left[ \frac{\partial}{\partial \vec{q}_1^2} (\epsilon_{L_c}^{*\beta'_1} \epsilon_{L_c}^{\beta_1} A_{0,\beta'_1}^* A_{0,\beta_1}) + \frac{1}{3} \Pi_1^{\alpha_1 \alpha_2} \epsilon_{L_c}^{*\beta'_1} \epsilon_{L_c}^{\beta_1} \text{Re} [A_{0,\beta'_1}^* A_{\alpha_1 \alpha_2, \beta_1}] \right] \Big|_{\vec{q}_1^2 = \vec{q}_2^2 = 0}, \end{cases} \quad (24)$$

1) The phase space integral element is expanded as  $d\phi_2 = \frac{|\vec{p}_1|}{32\pi^2 s^{3/2}} \frac{p_f}{p_i} d\Omega = d\phi_2^{(0)} [1 + f_{ps} * (|\vec{q}_1|^2 + |\vec{q}_2|^2) + O(v^4)]$ .

$$|N_2|^2 = \begin{cases} \left[ \frac{\partial}{\partial \bar{q}_2^2} (|A_{0,0}|^2) \right. \\ \left. + \frac{1}{3} \Pi_2^{\beta_1 \beta_2} \operatorname{Re}[A_{0,0}^* A_{0,\beta_1 \beta_2}] \right] \Big|_{\bar{q}_1^2 = \bar{q}_2^2 = 0}, \\ \left[ \frac{\partial}{\partial \bar{q}_2^2} (\epsilon_{L_c}^{*\beta'_1} \epsilon_{L_c}^{\beta_1} A_{0,\beta'_1}^* A_{0,\beta_1}) \right. \\ \left. + \frac{1}{15} \epsilon_{L_c}^{*\beta'_1} \Pi_2^{\beta_1 \beta_2 \beta_3} \operatorname{Re}[A_{0,\beta'_1}^* A_{0,\beta_1 \beta_2 \beta_3}] \right] \Big|_{\bar{q}_1^2 = \bar{q}_2^2 = 0}, \end{cases} \quad (25)$$

where the first and second rows of Eqs. (23)–(25) correspond to the production of double  $S$ -wave  $B_c$  mesons and " $S+P$ "-wave  $B_c$  mesons, respectively.

### III. INPUT PARAMETERS

We use the following input parameters in the numerical calculations [96, 97]

$$\begin{aligned} \alpha &= 1/137, m_c = 1.5 \text{ GeV}, m_b = 4.8 \text{ GeV}, m_Z = 91.1876 \text{ GeV}, \\ \Gamma_Z &= 2.4952 \text{ GeV}, \sin^2 \theta_w = 0.2312, v^2 = 0.15. \end{aligned} \quad (26)$$

$m_c, m_b$  represent the masses of charm and bottom quark, respectively;  $m_Z, \Gamma_Z$  are the mass and width of  $Z^0$  boson, respectively; and  $\theta_w$  is the Weinberg angle. The values of the square of the effective velocity  $v^2$  are estimated using [97]

$$v_i^2 = \frac{\langle T \rangle}{2\mu_H}, \quad \text{for } i = 1, 2, \quad (27)$$

where  $\langle T \rangle$  represents the averaged kinematic energy of quark inside the  $B_c$  meson and is estimated as 0.35 GeV, as reported in Ref. [98].

The values of the original wave functions have been reported in several Refs. [71, 83, 84, 97, 99]. Here, we use the set from Ref. [84],

$$|R_S(0)|^2 = 1.994 \text{ GeV}^3, |R'_P(0)|^2 = 0.3083 \text{ GeV}^5. \quad (28)$$

The matrix elements  $\langle v^2 \rangle$  adhere to the velocity power scaling rules and are of the order of  $v^2$  as

$$v^2 = \langle v^2 \rangle [1 + \mathcal{O}(v^4)]. \quad (29)$$

The running of strong coupling constant is taken at one-loop accuracy,

$$\alpha_s(\mu) = \frac{2\pi}{(11 - 2/3n_f) \ln(\mu/\Lambda_{\text{QCD}})} \quad (30)$$

with the active quark flavors  $n_f = 3$ ,  $\Lambda_{\text{QCD}} = 251 \text{ MeV}$ , and  $\alpha_s(m_Z) = 0.1184$ . In the subsequent calculations, we treat  $\alpha_s(\mu)$  as running with the collision energy  $\sqrt{s}$ , and we additionally quantify the uncertainties associated with the renormalization scale variation.

## IV. RESULTS AND DISCUSSION

### A. Cross section and differential cross section

Figure 1 shows the four types of processes, denoted as  $\gamma$ - $\gamma$ ,  $\gamma$ - $g$ ,  $Z$ - $\gamma$ , and  $Z$ - $g$ . These labels specify the nature of the two propagators in each process. The contributions from the pure electroweak (EW) diagrams ( $\gamma^*/Z^0$ - $\gamma$  type) are several orders of magnitude smaller than those from the QCD ( $\gamma^*/Z^0$ - $g$  type) diagrams. This suppression factors can be estimated by  $[Q_c Q_b \alpha / (C_F \alpha_s)]^2 \sim 10^{-4}$ , which arises from the coupling constants, charge of the heavy quark, and color factors. Thus, previous studies in Refs. [17–19, 69, 70] considered only QCD processes. Here, we do not show the results of the four types of processes ( $\gamma$ - $\gamma$ ,  $\gamma$ - $g$ ,  $Z$ - $\gamma$ , and  $Z$ - $g$ ); instead, we classify them into two types, *i.e.*,  $\gamma$ -propagated ( $\gamma$ - $\gamma$ ,  $\gamma$ - $g$ ) and  $Z^0$ -propagated ( $Z$ - $\gamma$ ,  $Z$ - $g$ ) processes. Consequently, we investigate the paired  $B_c$  production via  $\gamma^*/Z^0$ -propagators separately, as in Refs. [13, 17, 19], and we show the cross-sections as a function of the center-of-mass (c.m.) energy in Fig. 2. The  $\gamma$ -propagated processes are dominant in the low energy region, while the  $Z^0$ -propagated processes are dominant around the  $Z$ -factory energy region because of the resonance effect. Further, the interference between different mechanisms (*e.g.*, fragmentation and nonfragmentation [100]) can sometimes cause destructive contributions. Moreover, we calculated the interference contributions and found they were moderate, with the ratio  $(\sigma_{\text{total}} - \sigma_\gamma - \sigma_Z)/\sigma_{\text{total}}$  ranging from  $-5\%$  to  $5\%$ . In the following sections, we only discuss the total results (the sum of both processes, including the interference).

In contrast to Ref. [70], which studied the production of double  $S$ -wave  $B_c$  mesons via a virtual photon within the RQM, we present our results for the same mechanism within the NRQCD frame ( $s$ -channel  $\gamma$ - $g$  type) in Fig. 3. The NRQCD method yields results are qualitatively consistent with those in the RQM calculations, *i.e.*, the relativistic corrections have negative effects. The corresponding numerical cross-sections at  $\sqrt{s} = 22 \text{ GeV}$  are provided in Table 1.

The contributions of the  $t$ -channel double photon exchange have also been studied [71, 101]. We calculated the  $t$ -channel double photon production cross-sections and found that they were at least two orders of magnitude smaller than the corresponding  $s$ -channel cross-sections for all 11 processes considered herein. This is caused by a suppression factor of  $\alpha^2/\alpha_s^2$  ( $\sim 10^{-3}$ ). There-

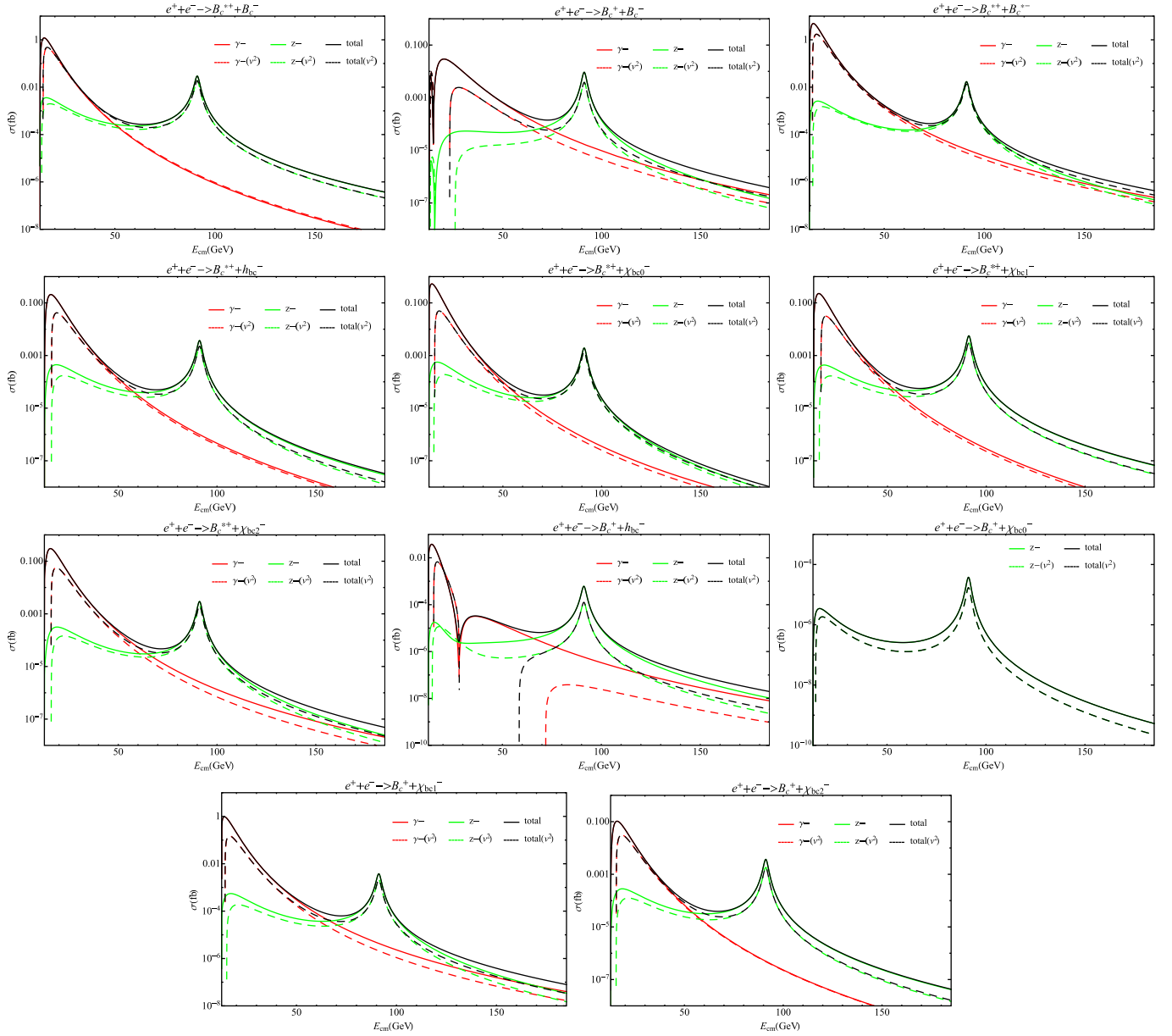


**Fig. 2.** (color online) Cross-section  $\sigma$  versus c.m. energy  $\sqrt{s}$  ( $E_{\text{cm}} = \sqrt{s}$ ). The red, green, and black lines correspond to  $\gamma$ -propagated processes,  $Z$ -propagated processes, and the sum of both, respectively. The solid line represents LO results, while the dashed line represents NLO( $v^2$ ) results.

fore, these contributions can be safely neglected. However, for comparison with Ref. [71], which studied the  $t$ -channel double-photon production mechanism within the RQM, we present our relativistic results for  $t$ -channel processes within the NRQCD frame in Fig. 3. Similar to the RQM results of Ref. [71], our study demonstrates that relativistic effects lead to negative corrections. The remaining differences may originate from distinct theoretical frameworks and input parameters (*e.g.*, quark masses and LDMEs). The numerical results at  $\sqrt{s} = 22$  GeV are presented in Table 1.

Furthermore, for  $B_c^+ + B_c^-$  production, Ref. [69] pro-

posed that higher-order contributions such as two-loop QCD corrections or relativistic corrections may resolve the problem of negative cross-sections observed in the next-to-leading order (NLO) QCD calculations. However, Fig. 3 shows that this issue persists even when relativistic corrections are included. Additionally, interferences between  $s$ - and  $t$ -channels were calculated and failed to resolve the problem.

The numerical results of cross sections for all processes are presented in Table 2, in which we list the cross sections for different renormalization scales at three energy points ( $m_Z/2, m_Z, 2m_Z$ ), for both LO and NLO in  $v^2$

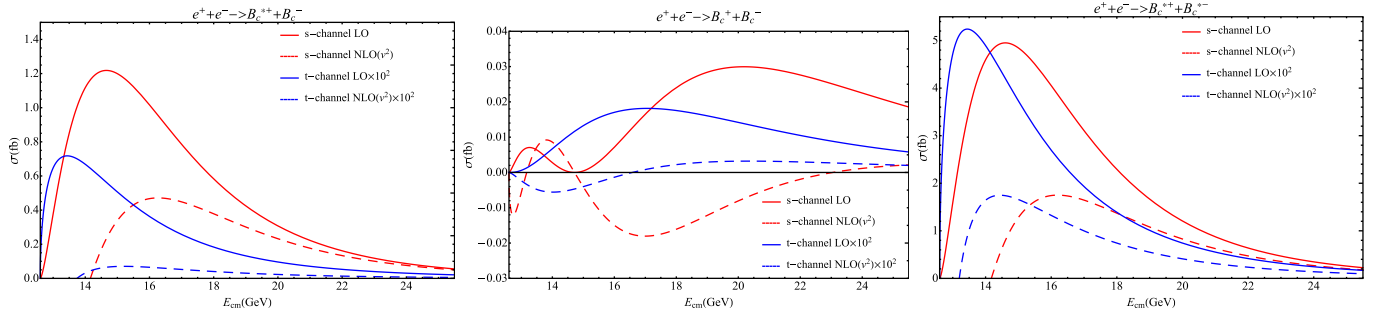


**Fig. 3.** (color online) Cross-section  $\sigma$  versus c.m. energy  $\sqrt{s}$  ( $E_{\text{cm}} = \sqrt{s}$ ) for the s-channel  $\gamma$ - $g$  type and t-channel processes. The red and blue lines represent s- and t-channel processes, respectively. The solid and dashed lines represent LO and NLO( $v^2$ ) results, respectively. The t-channel results are scaled up by a factor of 100.

**Table 1.** Production cross-sections of  $B_c^{*+} + B_c^-$ ,  $B_c^+ + B_c^-$ , and  $B_c^{*+} + B_c^{*-}$  production for the s-channel  $\gamma$ - $g$  type and t-channel double-photon processes. LO and NLO( $v^2$ ) indicate the leading order and next-to-leading order in the  $v^2$  expansions, respectively.

s-channel				
$\sqrt{s} = 22.0$ GeV	LO (this work)	NLO( $v^2$ ) (this work)	LO [70]	NLO ( $v^2$ ) [70]
$B_c^{*+} + B_c^-$	0.162 fb	0.133 fb	0.10 fb	0.04 fb
$B_c^+ + B_c^-$	0.028 fb	-0.002 fb	0.10 fb	0.03 fb
$B_c^{*+} + B_c^{*-}$	0.638 fb	0.472 fb	2.14 fb	0.58 fb
t-channel				
$\sqrt{s} = 22.0$ GeV	LO (this work)	NLO( $v^2$ ) (this work)	LO [71]	NLO ( $v^2$ ) [71]
$B_c^{*+} + B_c^-$	$0.53 \times 10^{-3}$ fb	$0.13 \times 10^{-3}$ fb	$0.18 \times 10^{-3}$ fb	$0.11 \times 10^{-3}$ fb
$B_c^+ + B_c^-$	$0.10 \times 10^{-3}$ fb	$0.03 \times 10^{-3}$ fb	$0.03 \times 10^{-3}$ fb	$0.02 \times 10^{-3}$ fb
$B_c^{*+} + B_c^{*-}$	$4.16 \times 10^{-3}$ fb	$2.35 \times 10^{-3}$ fb	$1.43 \times 10^{-3}$ fb	$0.46 \times 10^{-3}$ fb

expansions. The LO results are consistent with that in Ref. [69] when using the same input parameters<sup>1)</sup>. For  $B_c^+ + B_c^-$  production via the  $\gamma$ -propagator, the LO cross section takes a zero at an energy point  $s_0$  near the threshold or in the low energy region<sup>2)</sup>, and the value of  $s_0$  is obtained as follows,

$$s_0(B_c^+ + B_c^-) = \frac{2M^2(1 - 4r_c + 6r_c^2 - 4r_c^3 + 3r_c^4)}{r_c(1 - 3r_c + 5r_c^2 - 3r_c^3)}, \quad \sqrt{s_0} \approx 14.7 \text{ GeV}, \quad (31)$$

where  $r_c = m_c/M$ ,  $M = m_c + m_b$ , which is consistent with Ref. [69]. In contrast, for  $B_c^+ + h_{bc}^-$  production (via the  $\gamma$ -propagator), the LO cross-section at  $\sqrt{s} \approx 28.0$  GeV is not

strictly zero ( $\approx 1.3 \times 10^{-7}$  fb).

To examine the effects of the relativistic corrections, we plot the ratio  $\sigma_{\text{NLO}(v^2)}/\sigma_{\text{LO}}$  (*i.e.*, the  $K$ -factors) as a function of the collision energy in Fig. 4. Compared to the NLO QCD cross-sections, for which the  $K$ -factors are about 1.2–2.0 [69], the  $K$ -factors for the relativistic corrections are about 0.2–1.0. At high energies, the relativistic  $K$ -factors are  $\sim 0.6$ , indicating that relativistic corrections reduce the  $\mathcal{O}(v^0)$  cross-sections by about 40%. This level of suppression is expected and reasonable because it lies between the  $\sim 50\%$  reduction calculated for double charmonia production and  $\sim 20\%$  reduction for double bottomonia production [20]. In Appendix A, we present the ratios of the relativistic corrections to the LO SDCs in the high-energy limit, which also reflect the contributions of the relativistic corrections.

The production of double charmonia or double bottomonia is governed by numerous conservation laws [16, 20]. For example,  $C$ -parity conservation forbids processes such as  $e^+e^- \rightarrow 2J/\psi$ ,  $2\eta_c$ ,  $J/\psi + h_c$ ,  $\eta_c + \chi_c$  from proceeding via a  $\gamma^*$  propagator. Furthermore, a given process proceeds exclusively via either the vector or the axial-vector part of the  $Z^0$  current. For example,  $J/\psi + \eta_c$  production proceeds via the vector part, while  $\eta_c + \chi_c$  proceeds via the axial-vector part. For charged  $B_c$  mesons, these selection rules no longer hold. Consequently, we consider their  $P$ -parity properties. Weak interactions are known to violate  $P$ -parity; therefore, we define the  $P$ -asymmetry parameter  $\mathcal{A}$  following the definition in Ref. [69] as

$$\mathcal{A} = \langle \cos \theta \rangle = \frac{1}{\sigma} \int d\cos \theta \left[ \cos \theta \frac{d\sigma}{d\cos \theta} \right]. \quad (32)$$

For processes  $B_c^+ + B_c^-$  and  $B_c^+ + \chi_{bc0}^-$ , this asymmetry is

1) The difference between the cross sections presented herein and those in Ref. [69] stems from the choice of LDMEs. Specifically, Ref. [69] adopts the LDMEs for  $B_c$  mesons as  $\langle \mathcal{O} \rangle_{B_c} = \frac{M}{2} f_{B_c}^2$  with  $f_{B_c}^2 = 0.16 \text{ GeV}^2$ . The factor  $\langle \mathcal{O} \rangle_{B_c}/(2Nc)$  is the counterpart of  $|R_S(0)|^2/(4\pi)$  adopted in our calculations. This discrepancy in the LDME-related factors leads to a cross section ratio of  $\approx 0.3$ .

2) This dip behavior also appears in  $e^+e^- \rightarrow \gamma^*/Z^0 \rightarrow \chi_{Q0} + \gamma$  production [13, 102] due to an overall suppression factor of  $(s - 12m_Q^2)^2$ . For instance, taking  $m_Q = m_c = 1.5 \text{ GeV}$ , the corresponding energy point is  $\sqrt{s_0} \approx 5.2 \text{ GeV}$ .

**Table 2.** Production cross-sections at  $\sqrt{s} = m_Z/2, m_Z, 2m_Z$  for different renormalization scales. LO and NLO( $v^2$ ) indicate the leading and next-to-leading orders in the  $v^2$  expansions, respectively. The  $K$ -factor, defined as  $K = \sigma_{\text{NLO}(v^2)}/\sigma_{\text{LO}}$ , is identical across different scales  $\mu$ . Numerical results corresponding to the  $B_c^+ + \chi_{bc0}^-$  channel at  $\sqrt{s} = m_Z/2$  are not presented because their cross-sections ( $\sigma \sim 10^{-7}$  fb) are orders of magnitude smaller than those of the other processes, and the  $K$ -factor equals 0.54.

	$\mu = \sqrt{s}/2$		$\mu = \sqrt{s}$		$\mu = 2\sqrt{s}$		$\mu = 2M_{B_c}$		$K$
	LO	NLO( $v^2$ )	LO	NLO( $v^2$ )	LO	NLO( $v^2$ )	LO	NLO( $v^2$ )	
$\sqrt{s} = m_Z/2$	units: $\times 10^{-2}$ fb								
$B_c^{*+} + B_c^{*-}$	0.428	0.351	0.321	0.263	0.249	0.204	0.569	0.466	0.82
$B_c^{*+} + B_c^-$	0.113	0.107	0.085	0.080	0.066	0.062	0.151	0.142	0.94
$B_c^+ + B_c^-$	0.145	0.056	0.109	0.042	0.084	0.032	0.193	0.074	0.39
$B_c^{*+} + h_{bc}^-$	0.044	0.034	0.033	0.026	0.026	0.020	0.059	0.045	0.77
$B_c^{*+} + \chi_{bc0}^-$	0.033	0.022	0.025	0.016	0.019	0.013	0.044	0.029	0.67
$B_c^{*+} + \chi_{bc1}^-$	0.032	0.022	0.024	0.017	0.019	0.013	0.042	0.030	0.70
$B_c^{*+} + \chi_{bc2}^-$	0.060	0.040	0.045	0.030	0.035	0.023	0.080	0.053	0.67
$B_c^+ + h_{bc}^-$	0.0028	-0.0007	0.0021	-0.0005	0.0016	-0.0004	0.0037	-0.0009	-0.25
$B_c^+ + \chi_{bc1}^-$	0.083	0.048	0.062	0.036	0.048	0.028	0.011	0.064	0.58
$B_c^+ + \chi_{bc2}^-$	0.024	0.020	0.018	0.015	0.014	0.012	0.032	0.027	0.85
$\sqrt{s} = m_Z$	units: $\times 10^{-1}$ fb								
$B_c^{*+} + B_c^{*-}$	0.220	0.173	0.171	0.134	0.136	0.107	0.390	0.306	0.78
$B_c^{*+} + B_c^-$	0.379	0.242	0.294	0.188	0.235	0.150	0.672	0.429	0.64
$B_c^+ + B_c^-$	0.120	0.049	0.093	0.038	0.074	0.031	0.213	0.087	0.41
$B_c^{*+} + h_{bc}^-$	0.048	0.029	0.037	0.022	0.030	0.018	0.084	0.051	0.61
$B_c^{*+} + \chi_{bc0}^-$	0.025	0.018	0.019	0.014	0.015	0.011	0.044	0.032	0.74
$B_c^{*+} + \chi_{bc1}^-$	0.072	0.039	0.056	0.030	0.045	0.024	0.128	0.069	0.54
$B_c^{*+} + \chi_{bc2}^-$	0.038	0.026	0.029	0.020	0.024	0.016	0.067	0.046	0.69
$B_c^+ + h_{bc}^-$	0.008	0.002	0.006	0.001	0.005	0.001	0.014	0.003	0.21
$B_c^+ + \chi_{bc0}^-$	0.0005	0.0002	0.0004	0.0002	0.0003	0.0001	0.0009	0.0004	0.45
$B_c^+ + \chi_{bc1}^-$	0.049	0.027	0.038	0.021	0.030	0.017	0.086	0.048	0.56
$B_c^+ + \chi_{bc2}^-$	0.048	0.024	0.037	0.018	0.029	0.015	0.084	0.042	0.50
$\sqrt{s} = 2m_Z$	units: $\times 10^{-6}$ fb								
$B_c^{*+} + B_c^{*-}$	0.594	0.390	0.474	0.312	0.387	0.255	1.355	0.890	0.66
$B_c^{*+} + B_c^-$	0.522	0.298	0.417	0.238	0.340	0.194	1.190	0.679	0.57
$B_c^+ + B_c^-$	0.673	0.309	0.523	0.240	0.417	0.192	1.192	0.547	0.46
$B_c^{*+} + h_{bc}^-$	0.046	0.022	0.037	0.018	0.030	0.014	0.105	0.050	0.48
$B_c^{*+} + \chi_{bc0}^-$	0.015	0.011	0.012	0.008	0.010	0.007	0.034	0.025	0.73
$B_c^{*+} + \chi_{bc1}^-$	0.096	0.046	0.077	0.036	0.063	0.030	0.219	0.104	0.48
$B_c^{*+} + \chi_{bc2}^-$	0.067	0.032	0.054	0.025	0.044	0.021	0.153	0.072	0.47
$B_c^+ + h_{bc}^-$	0.027	0.005	0.022	0.004	0.018	0.003	0.062	0.011	0.18
$B_c^+ + \chi_{bc0}^-$	0.0007	0.0003	0.0006	0.0003	0.0005	0.0002	0.0017	0.0007	0.43
$B_c^+ + \chi_{bc1}^-$	0.110	0.047	0.088	0.038	0.072	0.031	0.252	0.107	0.43
$B_c^+ + \chi_{bc2}^-$	0.060	0.023	0.048	0.018	0.039	0.015	0.137	0.053	0.38

exactly zero at all energies because the axial-vector part of the  $Z^0$  current ( $J^P = 1^+$ ) cannot produce two  $0^-$  states, and the vector part ( $J^P = 1^-$ ) cannot produce a  $0^- + 0^+$  state. Therefore, there is no V-A interference and no parity violation in these specific processes. For the same reason, the process  $B_c^+ + \chi_{bc0}^-$  ( $0^- + 0^+$ ) cannot proceed via a  $\gamma$ -propagator ( $J^P = 1^-$ ), as evident from Fig. 2. The asymmetry as a function of the collision energy is shown in Fig. 5. We find that the maximal asymmetry occurs at  $\sqrt{s} \approx m_Z/2$  and becomes nearly zero at the  $Z^0$  resonance peak. Specifically, the asymmetry vanishes at the following energy points for different processes,

$$\sqrt{s}(B_c^{*+} + B_c^{*-}) = 86.74 \text{ GeV}, \quad (33)$$

$$\sqrt{s}(B_c^{*+} + B_c^-) = 86.36 \text{ GeV}. \quad (34)$$

Another notable feature is that the relativistic corrections slightly enhance the asymmetry. Moreover, we note that the azimuthal asymmetry  $\langle \cos\theta \rangle$  becomes nearly zero for all production processes at sufficiently high collision energies. For instance, in  $B_c^{*+} + \chi_{bcJ}^-$  production, this beha-

avior occurs at  $\sqrt{s} \geq 1000$  GeV. The angular distributions  $d\sigma/d\cos\theta$  for three energy points ( $\sqrt{s} = m_Z/2, m_Z, 2m_Z$ ) are shown in Fig. 6, where  $\theta$  is the angle between momenta of the electron ( $k_1$ ) and the meson  $H_1$  ( $p_1$ ). The distributions are consistent with the azimuthal asymmetry results shown in Fig. 5. Specifically, the more symmetric the angular distribution, the closer the azimuthal asymmetry is to zero, and vice versa. Owing to the existence of the V-A interference term, the angular distributions of all processes except for  $B_c^+ + B_c^-$  and  $B_c^+ + \chi_{bc0}^-$  processes are asymmetric and correlate with the azimuthal asymmetry, and are generally described by a three-parameter functional form given by  $d\sigma/d\cos\theta = A + B\cos\theta + C\cos^2\theta$ . This form exhibits distinct behavior relative to that of double heavy quarkonium production in the s-channel, which obeys the trivial functional form given by  $d\sigma/d\cos\theta = A(1 + B\cos^2\theta)$ [20, 103, 104].<sup>1)</sup>

The transverse momentum distribution  $\frac{d\sigma}{dp_t}$  can be written as

$$\frac{d\sigma}{dp_t} = \left| \frac{d\cos\theta}{dp_t} \right| \frac{d\sigma}{d\cos\theta} = \frac{p_t}{|p_1| \sqrt{p_1^2 - p_t^2}} \frac{d\sigma}{d\cos\theta}, \quad (35)$$

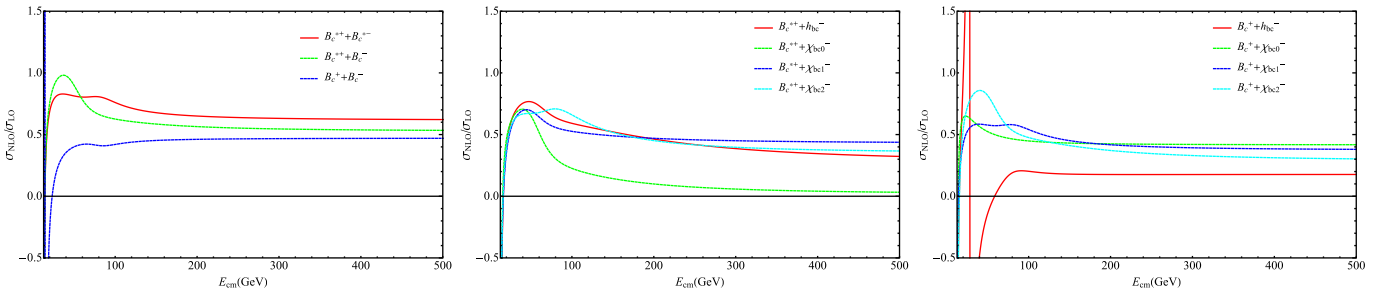


**Fig. 4.** (color online)  $\sigma_{\text{NLO}(\nu^2)}/\sigma_{\text{LO}}$  versus c.m. energy. The left, middle, and right panels correspond to the production of double S-wave  $B_c$  meson,  $B_c^{*+} + X$ , and  $B_c^+ + X$ , respectively, where  $X$  denotes  $h_{bc}^-$  or  $\chi_{bcJ}^-$  ( $J = 0, 1, 2$ ).

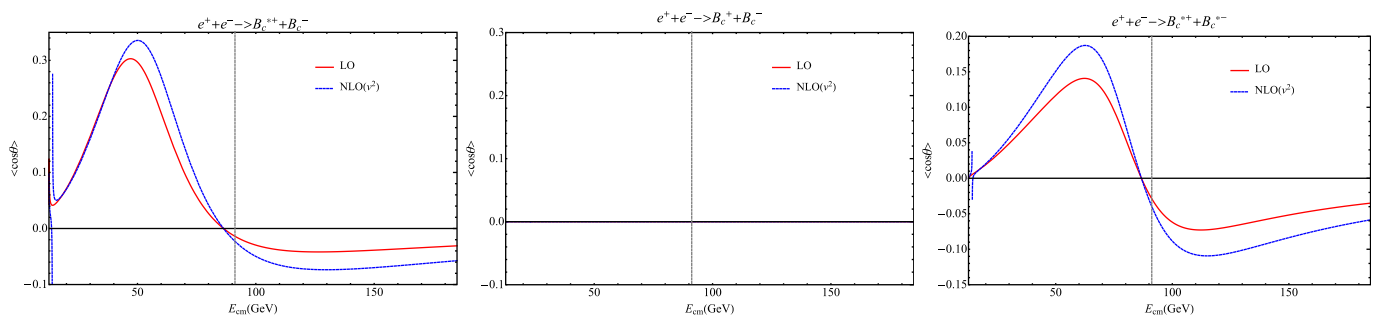


**Fig. 5.** (color online) Azimuthal asymmetry versus c.m. energy. The red solid and blue dashed lines represent the LO and NLO( $\nu^2$ ) results, respectively. The vertical dashed line marks  $\sqrt{s} = m_Z$ . The asymmetry is exactly zero for  $B_c^+ + B_c^-$  production.

1) For  $t$ -channel production processes, the angular distributions generally exhibit non-trivial behavior. A prototypical example is the production of double  $\eta_Q$  mesons, whose angular distribution is given by:  $d\sigma/d\cos\theta = A\cos^2\theta(1 + B\cos^2\theta)$ [20]. For the  $t$ -channel production of  $B_c^+ + B_c^-$  and  $B_c^{*+} + B_c^{*-}$  pairs, the corresponding angular distributions take distinct functional forms: the former follows the same form as the double  $\eta_Q$  meson production, while the latter is described by  $d\sigma/d\cos\theta = A + B(C + \cos^2\theta)^2$ . Nevertheless, as noted earlier, the total angular distributions of  $B_c$  meson production processes are dominated by the contributions of s-channel processes.

where the momentum of the  $H_1$  meson is given by

$$p_1 = \frac{\sqrt{\lambda[s, (E_c + E_b)^2, (E_b + E_c)^2]}}{2\sqrt{s}},$$

$$\lambda[x, y, z] = x^2 + y^2 + z^2 - 2(xy + yz + zx). \quad (36)$$

Combining Eqs. (35) and (36), we can also get an  $\mathcal{O}(v^2)$  expression,

$$\frac{d\sigma}{dp_t} = \frac{4p_t[s(1-4r)(1-4r-4r_{p_t}) + 16m_b m_c(1-4r-2r_{p_t})v^2]}{s^2(1-4r)^{3/2}(1-4r-4r_{p_t})^{3/2}}$$

$$\times \frac{d\sigma}{d\cos\theta} + \mathcal{O}(v^4), \quad r_{p_t} = \frac{p_t^2}{s}. \quad (37)$$

Using the above expressions, we show the transverse momentum distributions  $d\sigma/dp_t$  at different c.m. energy points in Fig. 7.

### B. CO contributions

CO contributions are significant in annihilation and hadron production processes [48, 105]; however, they are relatively small in electron-positron collisions [20, 31] and some indirect production mechanisms [56, 59]. The contributions of CO states are significant in the high energy region for double heavy quarkonium production in electron-positron collisions, where the gluon fragmenta-

tion process is most important [20]. In contrast, there are no gluon fragmentation diagrams for the production of paired  $B_c$  mesons.

The CO channels represent the inclusive processes for soft gluon emission or absorption. The complete calculations of LO inclusive production invoking CS+CO+g, CO+CO+g are of the NLO of  $\alpha_s$  compared with the CS channels. For CO pair channels in a special case, in which the two final states with an energy close to half of the c.m. energy recoil without the emission of additional light particles, those contribute to the exclusive CS double mesons production in the experimental measurements. This specific configuration leads to the breakdown of factorization caused by nonperturbative effects, which are fortunately suppressed by the inverse powers of the collision energy and usually negligible. To obtain a rough estimate of these contributions, we follow the velocity scaling rules of NRQCD and the approach used in Refs. [31, 48, 56, 57, 59, 105], assuming a relationship between the CO and CS LDMEs.

$$\langle \mathcal{O}_8^H \rangle \simeq \Delta_S(v)^2 \langle \mathcal{O}_1^H \rangle. \quad (38)$$

Here,  $\Delta_S(v)$  is of order  $v^2$ , with typical values  $v^2 \sim 0.1-0.3$ , and  $\Delta_S(v) \sim \alpha_s(M_{B_c}v)$ .

We now estimate the CO contribution to the cross-section at the  $Z^0$  peak. As noted previously, the electroweak contributions are several orders of magnitude smaller than the QCD contributions, and therefore, it is

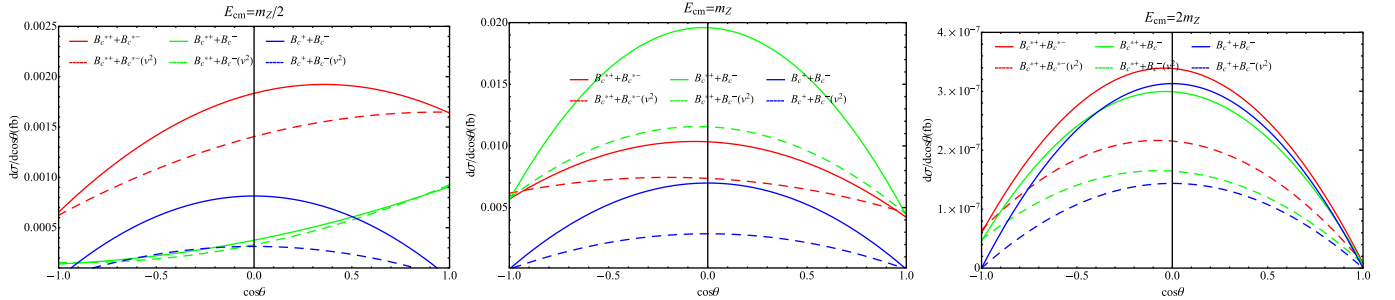


**Fig. 6.** (color online) Differential cross section  $d\sigma/d\cos\theta$  at different c.m. energy. The left, middle and right panels correspond to  $\sqrt{s} = m_Z/2$ ,  $\sqrt{s} = m_Z$ , and  $\sqrt{s} = 2m_Z$ , respectively. The solid line represents LO results and the dashed line represents NLO( $v^2$ ) results.

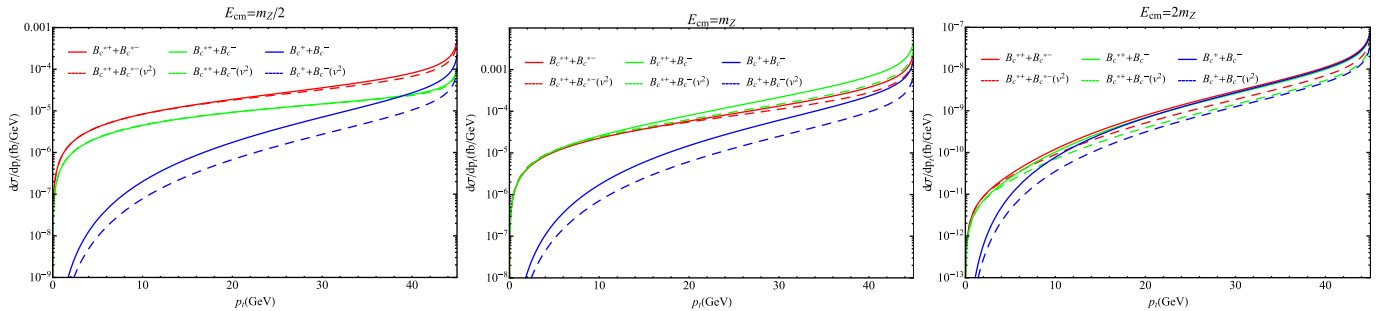


**Fig. 7.** (color online) Differential cross-section  $d\sigma/dp_t$  at different c.m. energies. The left, middle, and right panels correspond to  $\sqrt{s} = m_Z/2$ ,  $\sqrt{s} = m_Z$ , and  $\sqrt{s} = 2m_Z$ , respectively. The solid and dashed lines represent the LO and NLO( $v^2$ ) results, respectively.

sufficient to consider only  $\gamma/Z$ - $g$  type processes. The color factor for the CS amplitude squared is  $|C_s|^2 = C_F^2$ , while for the CO one it is  $|C_o|^2 = C_F/(2N_c)$ . The CO cross-section is related to the CS cross-section as

$$\sigma_8 = \sigma_1 \times \frac{|C_o|^2}{|C_s|^2} \times v^8 = \sigma_1 \times \frac{v^8}{8}. \quad (39)$$

Taking  $v^2 = 0.15$  and considering  $B_c^{*+} + B_c^-$  production (via  ${}^3S_1^{[1]} + {}^1S_0^{[1]}$ ) as an example, the CS cross-section at the  $Z^0$  peak is 0.030 fb. The four main CO channels are  ${}^3S_1^{[8]} + {}^1S_0^{[8]}$ ,  ${}^3S_1^{[8]} + {}^3S_1^{[8]}$ ,  ${}^1S_0^{[8]} + {}^3S_1^{[8]}$ , and  ${}^1S_0^{[8]} + {}^1S_0^{[8]}$ . The total CO cross section is then estimated as

$$\sigma_8 \simeq 4 \times \sigma_1 \times \frac{v^8}{8} \simeq 7.6 \times 10^{-6} \text{ fb}. \quad (40)$$

This is approximately three orders of magnitude smaller

than the CS contribution.

### C. Uncertainties

Theoretical uncertainties in our calculation arise from several sources, including the LDMEs, heavy quark masses, and the choice of renormalization scale.

For the LDMEs, various studies [51, 71, 83, 84, 97, 99] report values in the ranges  $|R_S(0)|^2 \in (1.30, 6.21)$  and  $|R'_P(0)|^2 \in (0.16, 0.90)$ . Based on these ranges, we estimate that the LDMEs can introduce uncertainties of approximately  $-57\%$  to  $+870\%$  for double  $S$ -wave  $B_c$  production, and  $-66\%$  to  $+809\%$  for " $S+P$ " waves  $B_c$  pair production.

The renormalization scale uncertainty is partially illustrated in Table 2. At  $\sqrt{s} = m_Z$ , the dependence on the scale is similar to that observed in double heavy quarkonium production (*cf.* Figs. 10 and 11 in Ref. [20]): it decreases with increasing collision energy and leads to

**Table 3.** Uncertainties for the total cross-sections at  $\sqrt{s} = m_Z$  with varying  $m_c$ , where  $m_b$  is fixed to 4.8 GeV.

$\sigma(\times 10^{-1} \text{ fb})$	$m_c = 1.2 \text{ GeV}$		$m_c = 1.5 \text{ GeV}$		$m_c = 1.8 \text{ GeV}$	
	LO	NLO( $v^2$ )	LO	NLO( $v^2$ )	LO	NLO( $v^2$ )
$B_c^{*+} + B_c^{*-}$	0.425	0.311	0.171	0.134	0.085	0.071
$B_c^{*+} + B_c^-$	0.649	0.373	0.294	0.188	0.162	0.113
$B_c^+ + B_c^-$	0.198	0.066	0.093	0.038	0.052	0.025
$B_c^{*+} + h_{bc}^-$	0.149	0.080	0.037	0.022	0.012	0.008
$B_c^{*+} + \chi_{bc0}^-$	0.073	0.046	0.019	0.014	0.007	0.006
$B_c^{*+} + \chi_{bc1}^-$	0.183	0.084	0.056	0.030	0.023	0.014
$B_c^{*+} + \chi_{bc2}^-$	0.125	0.077	0.029	0.020	0.009	0.007
$B_c^+ + h_{bc}^-$	0.0194	0.0021	0.0061	0.0013	0.0024	0.0007
$B_c^+ + \chi_{bc0}^-$	0.0021	0.0007	0.0004	0.0002	0.00008	0.00005
$B_c^+ + \chi_{bc1}^-$	0.134	0.066	0.038	0.021	0.014	0.009
$B_c^+ + \chi_{bc2}^-$	0.142	0.061	0.037	0.018	0.012	0.007

**Table 4.** Uncertainties for the total cross-sections at  $\sqrt{s} = m_Z$  with varying  $m_b$ , where  $m_c$  is fixed to 1.5 GeV.

$\sigma(\times 10^{-1} \text{ fb})$	$m_b = 4.4 \text{ GeV}$		$m_b = 4.8 \text{ GeV}$		$m_b = 5.2 \text{ GeV}$	
	LO	NLO( $v^2$ )	LO	NLO( $v^2$ )	LO	NLO( $v^2$ )
$B_c^{*+} + B_c^{*-}$	0.137	0.108	0.171	0.134	0.215	0.168
$B_c^{*+} + B_c^-$	0.254	0.166	0.294	0.188	0.344	0.216
$B_c^+ + B_c^-$	0.085	0.038	0.093	0.038	0.102	0.039
$B_c^{*+} + h_{bc}^-$	0.028	0.017	0.037	0.022	0.049	0.029
$B_c^{*+} + \chi_{bc0}^-$	0.014	0.011	0.019	0.014	0.026	0.018
$B_c^{*+} + \chi_{bc1}^-$	0.049	0.028	0.056	0.030	0.065	0.034
$B_c^{*+} + \chi_{bc2}^-$	0.022	0.015	0.029	0.020	0.039	0.027
$B_c^+ + h_{bc}^-$	0.0057	0.0014	0.0061	0.0013	0.0065	0.0011
$B_c^+ + \chi_{bc0}^-$	0.00026	0.00013	0.00038	0.00017	0.00052	0.00021
$B_c^+ + \chi_{bc1}^-$	0.031	0.018	0.038	0.021	0.047	0.026
$B_c^+ + \chi_{bc2}^-$	0.030	0.015	0.037	0.018	0.046	0.022

variations of  $\sim -20\%$  (for  $\mu = 2m_Z$ ) to  $+128\%$  (for  $\mu = 2M_{B_c}$ ). For simplicity, these are not explicitly shown in the figures.

To quantify the uncertainties from the heavy quark masses, we adopt  $m_c = (1.5 \pm 0.3)$  GeV and  $m_b = (4.8 \pm 0.4)$  GeV, following Refs. [31, 58, 59]. The resulting total cross-sections at the  $Z^0$  pole are presented in Tables 3 and 4. These cross-sections are more sensitive to the charm quark mass, consistent with the previous findings [31, 58, 59]. Further, we find that the cross-sections increase with decreasing charm quark mass; however, its decrease with decreasing bottom quark mass. This behavior is similar to that seen for the  $(c\bar{b})_1[{}^3S_1, {}^3P_2]$  states in Refs. [31, 59]. In general, the uncertainty caused by the  $\pm 0.3$  GeV variation of charm quark mass is  $-40\% \sim +100\%$  for double  $S$ -wave  $B_c$  meson production and  $-60\% \sim +200\%$  for  $P$ -wave  $B_c$  meson-involved production processes, whereas that caused by the  $\pm 0.4$  GeV variation of bottom quark mass is  $-10\% \sim +10\%$  for double  $S$ -wave  $B_c$  meson production and  $-20\% \sim +20\%$  for  $P$ -wave  $B_c$  meson-involved production processes.

## V. CONCLUSIONS

Based on the previous studies of  $B_c$  meson pair production in  $e^+e^-$  collisions, including LO calculation [17–19], NLO QCD correction [69], and relativistic corrections within the RQM to both  $s$ -channel [70] and  $t$ -channel double-photon processes [71], we investigated the relativistic corrections to double  $B_c$  production in  $e^+e^-$  annihilation within the NRQCD factorization framework [1], calculating both  $\gamma^*$ - and  $Z^0$ -propagated processes, with c.m. energies ranging from the production threshold  $2M_{B_c}$  up to  $2m_Z$ .

The results confirm that the relativistic corrections are substantial, with  $K$ -factors of  $\sim 0.6$ , which correspond to a 40% reduction of the LO cross-sections. This effect is comparable in magnitude to the NLO QCD corrections, which have  $K$ -factors of  $\sim 1.4$  [69]. Further, we present the azimuthal asymmetry arising from  $P$ -parity violation as a function of the c.m. energy, along with the differential cross-sections (angular distribution and transverse momentum distribution) at specific energy points ( $m_Z/2$ ,  $m_Z$ , and  $2m_Z$ ). In addition, the theoretical uncertainties from quark masses and renormalization scale are discussed.

Considering the negligible contributions from the  $t$ -channel double-photon mechanism and CO states, the small reconstruction efficiency or decay branching fractions (*e.g.*,  $\mathcal{B}(B_c^\pm \rightarrow J/\psi\pi^\pm) \approx 0.5\%$  [106]), and the significant negative relativistic corrections, the observation of double  $B_c$  production remains challenging (as also poin-

ted out in Ref. [67]) for future  $ee$  collider  $Z$ -factory experiments despite the enhancing effect of NLO QCD corrections [69].

Therefore, alternative production modes may be more promising. These include operation near the production threshold ( $\sqrt{s} \sim 15$  GeV, a " $B_c^*$ -factory" [69]), or hadronic [41, 50, 51, 76] and photonic [41, 43, 44] production mechanisms. Finally, beyond QCD corrections for  $B_c$ -related processes, further calculation of relativistic corrections, which are relatively less studied, will be essential for gaining a deeper understanding of QCD and the properties of  $B_c$  mesons.

## APPENDIX A

We present the short-distance coefficient (SDC) ratios of the relativistic corrections (denoted as  $G$ ) relative to the LO ones (denoted as  $F$ ) for the processes  $e^+e^- \rightarrow Z^0/\gamma^* \rightarrow (c\bar{b})[{}^{2S_1+1}L_{1J_1}] + (b\bar{c})[{}^{2S_2+1}L_{2J_2}]$  in the high-collision energy limit ( $M^2 \ll s$ ). Further, we define  $R_i = G[n_i]/F[n_1 + n_2]$  (where  $n_i, i = 1, 2$  represent the final Fock states) and  $\xi = m_c/m_b$  in the following expressions. For the production of double  $S$ -wave states, we present the analytical expressions for different propagation processes:  $\gamma$ -propagator,  $Z^0$ -propagator, and the sum of the two processes including interference effects.

For  ${}^3S_1^{[1]} + {}^1S_0^{[1]}$  production, the  $Z^0$ -propagated process cross-section ratios are

$$R_1 = -\frac{11 - 12\xi + 6\xi^2 - 12\xi^3 + 11\xi^4}{3(1 + \xi)^2(1 + \xi^2)}, \quad (\text{A1})$$

$$R_2 = -\frac{11 - 4\xi + 6\xi^2 - 4\xi^3 + 11\xi^4}{3(1 + \xi)^2(1 + \xi^2)}. \quad (\text{A2})$$

The  $\gamma^*$ -propagated process cross-section ratios are

$$R_1 = -\frac{7 - 28\xi + 3\xi^2 - 6\xi^3 + 56\xi^4 - 14\xi^5}{3(1 + \xi)^2(1 - 2\xi^3)}, \quad (\text{A3})$$

$$R_2 = -\frac{7 - 32\xi + 3\xi^2 - 6\xi^3 + 64\xi^4 - 14\xi^5}{3(1 + \xi)^2(1 - 2\xi^3)}. \quad (\text{A4})$$

The total cross-section ratios are identical to those of the  $Z^0$ -propagated process Eqs. (A1) and (A2) because this process dominates overwhelmingly at high collision energies, and as shown in the first panel of Fig. 2, it is orders of magnitude larger than the  $\gamma^*$ -propagated process in the cross-section.

For  ${}^3S_1^{[1]} + {}^3S_1^{[1]}$  production,  $Z^0$ -propagated process cross section ratios,

$$R_1 = R_2 = \frac{3(11 - 12\xi + 6\xi^2 - 12\xi^3 + 11\xi^4) - 4(11 - 12\xi + 9\xi^2 - 24\xi^3 + 22\xi^4) \sin^2 \theta_w}{-9(1 + \xi)^2(1 + \xi^2) + 12(1 + \xi)^2(1 + 2\xi^2) \sin^2 \theta_w}, \quad (\text{A5})$$

The  $\gamma^*$ -propagated process cross-section ratios are

$$R_1 = R_2 = \frac{-22\xi^4 + 24\xi^3 - 9\xi^2 + 12\xi - 11}{3(\xi + 1)^2(2\xi^2 + 1)}. \quad (\text{A6})$$

The total cross-section ratios are

$$R_1 = R_2 = \left[ -9(1 + \xi^2)(11 - 12\xi + 6\xi^2 - 12\xi^3 + 11\xi^4) + 12(1 - \xi^2)(11 - 12\xi + 14\xi^2 - 12\xi^3 + 11\xi^4) \sin^2 \theta_w \right. \\ \left. - 8(11 - 12\xi + 31\xi^2 - 48\xi^3 + 67\xi^4 - 156\xi^5 + 143\xi^6) \sin^4 \theta_w \right] / \left[ 27(1 + \xi)^2(1 + \xi^2)^2 \right. \\ \left. - 36(1 - \xi^4)(1 + \xi)^2 \sin^2 \theta_w + 24(1 + \xi)^2(1 + 4\xi^2 + 13\xi^4) \sin^4 \theta_w \right]. \quad (\text{A7})$$

For  $^1S_0^{[1]} + ^1S_0^{[1]}$  production,  $Z^0$ -propagated process cross section ratios,

$$R_1 = R_2 = \frac{3(11 - 4\xi + 6\xi^2 - 4\xi^3 + 11\xi^4) - 4(11 - 4\xi + 9\xi^2 - 8\xi^3 + 22\xi^4) \sin^2 \theta_w}{-9(1 + \xi)^2(1 + \xi^2) + 12(1 + \xi)^2(1 + 2\xi^2) \sin^2 \theta_w}, \quad (\text{A8})$$

The  $\gamma^*$ -propagated process cross-section ratios are

$$R_1 = R_2 = \frac{-22\xi^4 + 8\xi^3 - 9\xi^2 + 4\xi - 11}{3(\xi + 1)^2(2\xi^2 + 1)}. \quad (\text{A9})$$

The total cross-section ratios are

**Table A1.** Ratios  $R$  for the process  $e^+e^- \rightarrow (c\bar{b})[^{2S_1+1}L_{1J_1}] + (b\bar{c})[^{2S_2+1}L_{2J_2}]$  in the high collision energy limit ( $M^2 \ll s$ ). The values are obtained by setting  $m_c = 1.5$  GeV,  $m_b = 4.8$  GeV.

	$\gamma^*$ -propagated		$Z^0$ -propagated		total	
	$R_1$	$R_2$	$R_1$	$R_2$	$R_1$	$R_2$
$B_c^{*+} + B_c^{*-}$	-1.23	-1.23	-1.39	-1.39	-1.28	-1.28
$B_c^{*+} + B_c^-$	0.24	0.48	-1.34	-1.82	-1.34	-1.82
$B_c^+ + B_c^-$	-1.72	-1.72	-1.87	-1.87	-1.76	-1.76
$B_c^{*+} + h_{bc}^-$	0.24	-1.15	-1.61	-3.22	-1.61	-3.22
$B_c^{*+} + \chi_{bc0}^-$	-0.21	-2.47	-0.48	-3.84	-0.23	-2.58
$B_c^{*+} + \chi_{bc1}^-$	-0.09	-1.19	-1.34	-2.47	-1.34	-2.47
$B_c^{*+} + \chi_{bc2}^-$	-1.55	-2.86	-1.48	-2.74	-1.53	-2.82
$B_c^+ + h_{bc}^-$	-2.28	-3.45	-2.02	-3.14	-2.17	-3.32
$B_c^+ + \chi_{bc0}^-$			-0.82	-3.08	-0.82	-3.08
$B_c^+ + \chi_{bc1}^-$	-1.72	-2.37	-1.87	-2.52	-1.76	-2.42
$B_c^+ + \chi_{bc2}^-$	1.03	-1.12	-1.99	-2.78	-1.99	-2.78
$t$ -channel double photon processes						
		$R_1$		$R_2$		
$B_c^{*+} + B_c^{*-}$		-0.89		-0.89		
$B_c^{*+} + B_c^-$		-0.89		-3.49		
$B_c^+ + B_c^-$		-1.37		-1.37		

$$\begin{aligned}
R_1 = R_2 = & [-9(1 + \xi^2)(11 - 4\xi + 6\xi^2 - 4\xi^3 + 11\xi^4) + 12(1 - \xi^2)(11 - 4\xi + 14\xi^2 - 4\xi^3 + 11\xi^4) \sin^2 \theta_w \\
& - 8(11 - 4\xi + 31\xi^2 - 16\xi^3 + 67\xi^4 - 52\xi^5 + 143\xi^6) \sin^4 \theta_w] / [27(1 + \xi)^2(1 + \xi^2)^2 - 36(1 - \xi^4) \\
& (1 + \xi)^2 \sin^2 \theta_w + 24(1 + \xi)^2(1 + 4\xi^2 + 13\xi^4) \sin^4 \theta_w].
\end{aligned} \tag{A10}$$

When  $m_c = m_b$  (*i.e.*  $\xi = 1$ ), these ratios are consistent with that in Refs. [20, 92–94].

For simplicity, we only show the numerical values of ratios  $R$  for other processes in Table A1.

## References

- [1] G. T. Bodwin, E. Braaten, and G. P. Lepage, *Phys. Rev. D* **51**, 1125 (1995) [Erratum: *Phys. Rev. D* **55**, 5853 (1997)]
- [2] Y. J. Zhang, Y. j. Gao, and K. T. Chao, *Phys. Rev. Lett.* **96**, 092001 (2006)
- [3] B. Gong and J. X. Wang, *Phys. Rev. D* **77**, 054028 (2008)
- [4] H. R. Dong, F. Feng, and Y. Jia, *Phys. Rev. D* **85**, 114018 (2012)
- [5] X. D. Huang, B. Gong, and J. X. Wang, *JHEP* **02**, 049 (2023)
- [6] F. Feng, Y. Jia, Z. w. Mo *et al.*, *Phys. Lett. B* **850**, 138506 (2024)
- [7] Z. G. He, Y. Fan, and K. T. Chao, *Phys. Rev. D* **75**, 074011 (2007)
- [8] Kazuo Abe *et al.*, *Phys. Rev. D* **70**, 071102 (2004)
- [9] Bernard Aubert *et al.*, *Phys. Rev. D* **72**, 031101 (2005)
- [10] M. y. Dong *et al.* CEPC Conceptual Design Report: Volume 2 - Physics & Detector, 11, (2018)
- [11] A. Abada *et al.*, *Eur. Phys. J. ST* **228**(2), 261 (2019)
- [12] C. H. Chang, J. X. Wang, and X. G. Wu, *Sci. China Phys. Mech. Astron.* **53**, 2031 (2010)
- [13] G. Chen, X. G. Wu, Z. Sun *et al.*, *Phys. Rev. D* **88**, 074021 (2013)
- [14] I. N. Belov, A. Berezhnoy, and E. Leshchenko, *Symmetry* **13**(7), 1262 (2021)
- [15] A. V. Berezhnoy, I. N. Belov, S. V. Poslavsky *et al.*, *Phys. Rev. D*, **104**, 034029 (2021)
- [16] I. N. Belov, A. V. Berezhnoy, and E. A. Leshchenko, *Phys. Atom. Nucl.* **86**(6), 1474 (2023)
- [17] Q. L. Liao, J. Jiang, and Y. H. Zhao, *Eur. Phys. J. C* **83**(1), 22 (2023)
- [18] Q. L. Liao and J. Jiang, *Chin. Phys. C* **48**(7), 073102 (2024)
- [19] Q. L. Liao and Y. Yu, *Eur. Phys. J. C* **84**(1), 1000 (2024)
- [20] X. P. Wang, G. Z. Xu, and K. Y. Liu, *Phys. Rev. D* **111**(11), 116007 (2025)
- [21] F. Abe *et al.*, *Phys. Rev. Lett.* **81**, 2432 (1998)
- [22] F. Abe *et al.*, *Phys. Rev. D* **58**, 112004 (1998)
- [23] R. Aaij *et al.*, *Phys. Rev. Lett.* **108**, 251802 (2012)
- [24] R. Aaij *et al.*, *Phys. Rev. Lett.* **120**(12), 121801 (2018)
- [25] R. Aaij *et al.*, *Phys. Rev. Lett.* **118**(11), 111803 (2017)
- [26] G. Aad *et al.*, *Eur. Phys. J. C* **76**(1), 4 (2016)
- [27] R. Aaij *et al.*, *Phys. Rev. Lett.* **111**(18), 181801 (2013)
- [28] Georges Aad *et al.*, *Phys. Rev. Lett.* **113**(21), 212004 (2014)
- [29] A. M. Sirunyan *et al.*, *Phys. Rev. Lett.* **122**(13), 132001 (2019)
- [30] R. Aaij *et al.*, *Phys. Rev. Lett.* **122**(23), 232001 (2019)
- [31] Z. Yang, X. G. Wu, G. Chen *et al.*, *Phys. Rev. D* **85**, 094015 (2012)
- [32] Z. Yang, X. G. Wu, and X. Y. Wang, *Comput. Phys. Commun.* **184**, 2848 (2013)
- [33] X. C. Zheng, C. H. Chang, and Z. Pan, *Phys. Rev. D* **93**(3), 034019 (2016)
- [34] X. C. Zheng, C. H. Chang, T. F. Feng *et al.*, *Sci. China Phys. Mech. Astron.* **61**(3), 031012 (2018)
- [35] X. C. Zheng, C. H. Chang, and T. F. Feng, *Sci. China Phys. Mech. Astron.* **63**(8), 281011 (2020)
- [36] Z. Y. Zhang, X. C. Zheng, and X. G. Wu, *Eur. Phys. J. C* **82**(3), 246 (2022)
- [37] Z. Yang, X. C. Zheng, and X. G. Wu, *Comput. Phys. Commun.* **281**, 108503 (2022)
- [38] K. Kolodziej, A. Leike, and R. Ruckl, *Phys. Lett. B* **348**, 219 (1995)
- [39] A. V. Berezhnoy, A. K. Likhoded, and M. V. Shevlyagin, *Phys. Lett. B* **342**, 351 (1995)
- [40] A. V. Berezhnoy, V. V. Kiselev, and A. K. Likhoded, *Phys. Lett. B* **381**, 341 (1996)
- [41] S. P. Baranov, *Phys. Rev. D* **55**, 2756 (1997)
- [42] G. Chen, X. G. Wu, H. B. Fu *et al.*, *Phys. Rev. D* **90**(3), 034004 (2014)
- [43] A. E. Dorokhov, R. N. Faustov, A. P. Martynenko *et al.*, *Phys. Rev. D* **102**(1), 016027 (2020)
- [44] Z. Q. Chen, H. Yang, and C. F. Qiao, *Phys. Rev. D* **102**(1), 016011 (2020)
- [45] H. Yang, Z. Q. Chen, and C. F. Qiao, *Phys. Rev. D* **105**(9), 094014 (2022)
- [46] C. H. Chang, Y. Q. Chen, G. P. Han *et al.*, *Phys. Lett. B* **364**, 78 (1995)
- [47] C. H. Chang, J. X. Wang, and X. G. Wu, *Phys. Rev. D* **70**, 114019 (2004)
- [48] C. H. Chang, C. F. Qiao, J. X. Wang *et al.*, *Phys. Rev. D* **71**, 074012 (2005)
- [49] C. H. Chang, C. F. Qiao, J. X. Wang *et al.*, *Phys. Rev. D* **72**, 114009 (2005)
- [50] R. Li, Y. J. Zhang, and K. T. Chao, *Phys. Rev. D* **80**, 014020 (2009)
- [51] Z. Q. Chen, L. B. Chen, and C. F. Qiao, *Phys. Rev. D* **109**(9), 096032 (2024)
- [52] A. V. Berezhnoy, V. V. Kiselev, and A. K. Likhoded, *Phys. Atom. Nucl.* **61**, 252 (1998)
- [53] Q. W. Hu, C. F. Qiao, and L. P. Sun, *Phys. Rev. D* **111**(9), 096003 (2025)
- [54] Y. p. Liu, C. Greiner, and A. Kostyuk, *Phys. Rev. C* **87**(1),

- 014910 (2013)
- [55] E. Norbeck, J. Nachtman, and Y. Onel, *J. Phys. Conf. Ser.* **458**, 012026 (2013)
- [56] C. H. Chang, J. X. Wang, and X. G. Wu, *Phys. Rev. D* **77**, 014022 (2008)
- [57] X. G. Wu, *Phys. Lett. B* **671**, 318 (2009)
- [58] L. C. Deng, X. G. Wu, Z. Yang *et al.*, *Eur. Phys. J. C* **70**, 113 (2010)
- [59] Z. Yang, X. G. Wu, L. C. Deng *et al.*, *Eur. Phys. J. C* **71**, 1563 (2011)
- [60] Q. L. Liao, X. G. Wu, J. Jiang *et al.*, *Phys. Rev. D* **85**, 014032 (2012)
- [61] Q. L. Liao, X. G. Wu, J. Jiang *et al.*, *Phys. Rev. D* **86**, 014031 (2012)
- [62] Q. L. Liao, Y. Yu, Y. Deng *et al.*, *Phys. Rev. D* **91**(11), 114030 (2015)
- [63] Q. L. Liao, Y. Deng, Y. Yu *et al.*, *Phys. Rev. D* **98**(3), 036014 (2018)
- [64] Q. L. Liao and J. Jiang, *Phys. Rev. D* **100**(5), 053002 (2019)
- [65] R. N. Faustov, F. A. Martynenko, and A. P. Martynenko, *Eur. Phys. J. A* **58**(1), 4 (2022)
- [66] I. N. Belov, A. V. Berezhnoy, A. E. Dorokhov *et al.*, *Nucl. Phys. A* **1015**, 122285 (2021)
- [67] Y. B. Wei, R. H. Li, D. Luo *et al.*, *Chin. Phys. C* **42**(8), 083107 (2018)
- [68] V. V. Kiselev, *Int. J. Mod. Phys. A* **10**, 465 (1995)
- [69] A. V. Berezhnoy, A. K. Likhoded, A. I. Onishchenko *et al.*, *Nucl. Phys. B* **915**, 224 (2017)
- [70] A. A. Karyasov, A. P. Martynenko, and F. A. Martynenko, *Nucl. Phys. B* **911**, 36 (2016)
- [71] A. V. Berezhnoy, A. P. Martynenko, F. A. Martynenko *et al.*, *Nucl. Phys. A* **986**, 34 (2019)
- [72] D. Ebert, R. N. Faustov, and V. O. Galkin, *Phys. Rev. D* **67**, 014027 (2003)
- [73] A. P. Martynenko, *Phys. Rev. D* **72**, 074022 (2005)
- [74] D. Ebert and A. P. Martynenko, *Phys. Rev. D* **74**, 054008 (2006)
- [75] J. Lee, W. L. Sang, and S. Kim, *JHEP* **01**, 113 (2011)
- [76] A. M. Trunin and A. P. Martynenko, *PoS BaldinISHEPPXXII*, 118 (2015)
- [77] R. I. Zhu, Y. Ma, X. L. Han *et al.*, *Phys. Rev. D* **95**(9), 094012 (2017)
- [78] W. Wang, J. Xu, D. s. Yang *et al.*, *JHEP* **12**, 012 (2017)
- [79] R. I. Zhu, *Nucl. Phys. B* **931**, 359 (2018)
- [80] Z. K. Geng, T. h. Wang, Y. Jiang *et al.*, *Phys. Rev. D* **99**(1), 013006 (2019)
- [81] D. s. Yang and W. j. Zhang, *Chin. Phys. C* **43**(8), 083101 (2019)
- [82] E. J. Eichten and C. Quigg, *Phys. Rev. D* **49**, 5845 (1994)
- [83] Q. L. Liao and G. Y. Xie, *Phys. Rev. D* **90**(5), 054007 (2014)
- [84] E. J. Eichten and C. Quigg, *Phys. Rev. D* **99**(5), 054025 (2019)
- [85] N. Brambilla, A. Pineda, J. Soto *et al.*, *Nucl. Phys. B* **566**, 275 (2000)
- [86] G. T. Bodwin and A. Petrelli, *Phys. Rev. D* **66**, 094011 (2002)
- [87] G. T. Bodwin, H. S. Chung, D. Kang *et al.*, *Phys. Rev. D* **77**, 094017 (2008)
- [88] H. K. Guo, Y. Q. Ma, and K. T. Chao, *Phys. Rev. D* **83**, 114038 (2011)
- [89] G. T. Bodwin, J. Lee, and E. Braaten, *Phys. Rev. D* **67**, 054023 (2003) [Erratum: *Phys. Rev. D* **72**, 099904 (2005)]
- [90] S. Bhatnagar and H. Negash, *Nucl. Phys. A* **1053**, 122969 (2025)
- [91] Z. G. He, Y. Fan, and K. T. Chao, *Phys. Rev. D* **81**, 054036 (2010)
- [92] G. Z. Xu, Y. J. Li, K. Y. Liu *et al.*, *Phys. Rev. D* **86**, 094017 (2012)
- [93] Y. J. Li, G. Z. Xu, K. Y. Liu *et al.*, *JHEP* **07**, 051 (2013)
- [94] G. Z. Xu, Y. J. Li, K. Y. Liu *et al.*, *JHEP* **10**, 071 (2014)
- [95] A. Petrelli, M. Cacciari, M. Greco *et al.*, *Nucl. Phys. B* **514**, 245 (1998)
- [96] S. Navas *et al.*, *Phys. Rev. D* **110**(3), 030001 (2024)
- [97] A. V. Berezhnoy, I. N. Belov, and A. K. Likhoded, *Phys. Rev. D* **103**(11), 114001 (2021)
- [98] S. S. Gershtein, V. V. Kiselev, A. K. Likhoded *et al.*, *Phys. Usp.* **38**, 1 (1995)
- [99] D. Ebert, R. N. Faustov, and V. O. Galkin, *Eur. Phys. J. C* **71**, 1825 (2011)
- [100] J. I. Lu, C. P. Jia, Y. Jia *et al.*, *Phys. Rev. D* **109**(9), 094022 (2024)
- [101] H. Negash, *Int. J. Mod. Phys. E* **34**(06), 2550015 (2025)
- [102] Q. L. Liao, J. Jiang, P. C. Lu *et al.*, *Phys. Rev. D* **105**(1), 016026 (2022)
- [103] K. Y. Liu, Z. G. He, and K. T. Chao, *Phys. Rev. D* **77**, 014002 (2008)
- [104] W. L. Sang, F. Feng, Y. Jia *et al.*, *Phys. Lett. B* **843**, 138057 (2023)
- [105] X. G. Wu, C. H. Chang, Y. Q. Chen *et al.*, *Phys. Rev. D* **67**, 094001 (2003)
- [106] C. H. Chang and Y. Q. Chen, *Phys. Rev. D* **49**, 3399 (1994)